PAPER

Check for updates

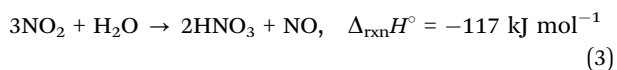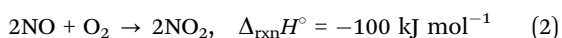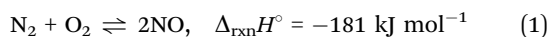# Mechanisms for sonochemical oxidation of nitrogen†

Thomas Qureishy,[ab] Sverre Løyland, [ID][ac] Susanne J. Jørgensen,[ad] Eline M. Færgestad,[ad] Truls Norby[ab] and Einar Uggerud*[ac]

N_2O, and mixtures of N_2 and O_2, dissolved in water—both in the presence and absence of added noble gases—have been subjected to ultrasonication with quantification of nitrite and nitrate products. Significant increase in product formation upon adding noble gas for both reactant systems is observed, with the reactivity order Ne < Ar < Kr < Xe. These observations lend support to the idea that extraordinarily high electronic and vibrational temperatures arise under these conditions. This is based on recent observations of sonoluminescence in the presence of noble gases and is inconsistent with the classical picture of adiabatic bubble collapse upon acoustic cavitation. The reaction mechanisms of the first few reaction steps necessary for the critical formation of NO are discussed, illustrated by quantum chemical calculations. The role of intermediate N_2O in this series of elementary steps is also discussed to better understand the difference between the two reactant sources (N_2O and $2:1\ N_2:O_2$; same stoichiometry).
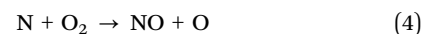
Introduction

Nitrate is the main ingredient in agricultural fertilizers. Today, its industrial production incorporates two coupled processes: the formation of ammonia from nitrogen and hydrogen (Haber process) followed by the oxidation of the ammonia to nitric acid (Ostwald process).[1] In principle, a one-step process, avoiding the energetically unfavorable intermediate ammonia, using only nitrogen, oxygen and water as feedstock, would be more attractive. In fact, such a process, the Birkeland–Eyde process,[2–5] involving nitric oxide (NO) and nitrogen dioxide (NO_2) as intermediates does exist:

$$N_2 + O_2 \rightleftharpoons 2NO, \quad \Delta_{rxn}H^\circ = -181 \text{ kJ mol}^{-1} \quad (1)$$

$$2NO + O_2 \rightarrow 2NO_2, \quad \Delta_{rxn}H^\circ = -100 \text{ kJ mol}^{-1} \quad (2)$$

$$3NO_2 + H_2O \rightarrow 2HNO_3 + NO, \quad \Delta_{rxn}H^\circ = -117 \text{ kJ mol}^{-1} \quad (3)$$

This was the preferred industrial method during the first two decades of the 20th century. The Birkeland–Eyde process has its origin in the late 18th century, when Cavendish studied the effect of an electric discharge on air and identified the

a Department of Chemistry, University of Oslo, Norway.
  E-mail: einar.uggerud@kjemi.uio.no

b Centre for Materials Science and Nanotechnology, University of Oslo, Norway

c Hylleraas Centre for Quantum Molecular Sciences, University of Oslo, Norway

d Centre for Biogeochemistry in the Anthropocene, University of Oslo, Norway

† Electronic supplementary information (ESI) available. See DOI: https://doi.org/10.1039/d2cp01995g

formation of oxidized nitrogen.[6] It should also be noted that the chemical reactions outlined above also occur during lightning, which provides a substantial amount of natural fertilization of Earth.[7] The Birkeland–Eyde process was soon outcompeted by the overall more economical Haber–Ostwald process, despite the former's intuitive quality of being direct. The key step in the Birkeland–Eyde process is the first, endothermic formation of nitric oxide (eqn (1)), in which the energy is provided by an enormous magnetically enhanced electric plasma discharge reactor, where atomization of N_2 and O_2 is achieved. The so-called Zel'dovich reactions,[8–10]

$$N + O_2 \rightarrow NO + O \quad (4)$$

and

$$O + N_2 \rightarrow NO + N, \quad (5)$$
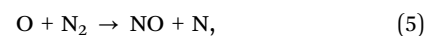
are traditionally applied to account for NO production in plasmas.

NO formation (1) becomes thermodynamically more favorable the higher the temperature is. However, produced NO starts to dissociate when the temperature becomes too high, and $T = 3200$ K is considered an optimum.[9] The second step, further oxidation to give NO_2 (2) is exothermic and occurs in the colder zone outside the high temperature plasma. In practice, the yield of NO + NO_2 (NO_x) in the Birkeland–Eyde process is only a few per cent per reaction cycle, thereby limiting the energy efficiency. For this reason, finding alternative, direct ways to nitrogen oxidation are desirable, considering that

This journal is © the Owner Societies 2022

Phys. Chem. Chem. Phys., 2022, **24**, 15357–15364 | 15357

NO and NO$_2$ production have opposite thermodynamic requirements.

Sonochemistry may provide such an alternative. It is now well established that during acoustic cavitation resulting from intense ultrasound radiation of a solution, plasma-like conditions exist transiently upon sudden bubble collapse, with local temperatures and pressure exceeding 5000 K and 100 kbar.[11] More recently, systematic observations of sonoluminescence indicate even higher temperatures, up to 20 000 K, with subsequent cooling rates exceeding 10^{12} K s^{-1}.[12] Altogether, this provides in principle an opportunity for NO production upon bubble collapse directly followed by oxidation to NO$_2$ as the temperature lowers.

On this background it is not surprising to find that sonochemical production of nitrite and nitrate from air dissolved in water has been studied and is well documented in the literature. As early as in 1936, Schultes and Gohr determined by colorimetry and iodometry the production of H$_2$O$_2$, nitrous acid and nitric acid as products after applying ultrasound to air-saturated water.[13] They found that NO was produced first and was further oxidized to NO$_2$ if there was enough oxygen present. Further studies have been performed by several research groups. For instance, Virtanen and co-workers reported that hydrogen gas and carbon monoxide prevent nitrogen fixation and that the total production was pH-independent.[14,15] Furthermore, it has been reported that dissolved O$_2$ rather than H$_2$O is the dominant source of oxygen for both NO and NO$_2$.[8,16-18]

Henglein and co-workers conducted a series of experiments where Ar was added as an inert gas to gas mixtures dissolved in water for sonochemistry. The relative amount of Ar was observed to influence sonochemical nitrate and nitrite production in reactions of nitrous oxide (N$_2$O)[19,20] and N$_2$,[21] respectively, and in the formation of H$_2$O$_2$ upon addition of O$_2$.[22] Interestingly, in the presence of O$_2$ the authors noticed the formation of more nitrite and nitrate indicating an "O" + N$_2$O pathway for NO production. In neither of these papers was any active role of Ar mentioned other than it could reduce the cooling rate having a lower heat capacity ratio than the other gases.

Suslick et al. have reported optical emission in bubble cavitation experiments of concentrated sulfuric acid containing noble gases and noted the presence of both highly excited neutral noble gas atoms and ions, with intensities and spectral widths only compatible with non-thermal plasmas comprising energetic particles that give rise to electron impact dissociation and ionization, and bremsstrahlung.[12,23-25] Nikitenko and co-workers compared OH emission spectra of water saturated with Ar and Xe, and concluded that the electronic and vibrational temperatures of the OH radicals in Xe are significantly higher than in Ar.[26,27] They suggested that a lower ionization energy of Xe provides a plasma with higher free electron density and temperature, and that collisions of electrons with water molecules to give excited OH radicals therefore are more effective in Xe. An alternative explanation could be that Xe is more soluble, thereby creating more bubbles. In a following review paper[28]

the same authors write without literature citation that "it has been known for a long time that heavy noble gases like Xe and Kr result in more OH radicals than lighter noble gases such as He, Ne and Ar."

The purpose of our work is fourfold. First, partly reproducing the previously mentioned experiments, we wanted to investigate how nitrate and nitrite production depend on the O$_2$: N$_2$ ratio in the sonochemical version of the Birkeland–Eyde process. Second, since it has been suggested that there is an "O" + N$_2$O pathway towards NO, we wanted to conduct separate experiments with N$_2$O as feedstock. Third, we considered it useful to analyze the experimental data using reaction models firmly based on quantum chemical calculations to shed light on the key reaction steps with emphasis on the role of N$_2$O as an intermediate in the production of NO. In this, we humbly realize the inherent complexity of the plasma chemistry at work. Fourth and finally, it would be interesting to investigate how nitrate/nitrite formation is affected by the presence and nature of added noble gas, with reference to the assumption of Nikitenko that the formation of OH radicals (or similar reactive species) increases down the group of the noble gases (Ne–Xe).[28]

Materials and methods

Experimental

Ultrasound was applied for an hour to 150 mL liquid samples of type-II water using a Hielscher UIP1000hdT-230 ultrasonic processor, which consists of a transducer connected to a generator, and has a frequency of 20 kHz and maximum power of 1 kW. The sonotrode in contact with the liquid in the reactor had a diameter of 34 mm, and between the transducer and sonotrode was a booster horn, amplifying the signal by a factor of 2.2. The processor was set to power mode, which keeps the power stable, as opposed to amplitude mode, which keeps the amplitude stable. The power was set to 80% of the maximum value. The total power and net power dissipated into the sample were around 400 and 270 W, respectively, and were recorded continuously. The sample chamber was water-cooled to stay at temperatures within 21–26 °C. The temperature was measured by a TF100 thermocouple before and after the ultrasonication.

The reactor has an arm above the level of the liquid sample. This arm was closed with a small septum. Two needles were inserted through the septum, of which one is for gas insertion. Outside the reactor it is connected with a Swagelok fitting to a 1/8 inch diameter stainless steel tube, and inside the reactor it is bent downwards and immersed deep into the liquid, so that gas is inserted near the bottom surface, providing maximum contact with and possibility to dissolve in the liquid. The other needle allows for gas to escape the reactor. It is straight and its end inside the reactor is therefore above the sample surface. In the experiments reported here, water-cooling was started one minute before turning on the ultrasound.

A stable gas flow was kept at 100 sccm (mL$_N$ min^{-1}) for 15 minutes before applying the ultrasound and then for 1 h during ultrasonication. The gas mixtures and flow were

15358 | *Phys. Chem. Chem. Phys.*, 2022, **24**, 15357–15364

This journal is © the Owner Societies 2022

manually controlled using calibrated variable-area rotameters with precision needle valves. Four sets of experiments were carried out (see Table S1 in ESI†). In the first, the gas mixtures consisted of nitrogen and oxygen, to check for consistency with literature data. In the second set of experiments, N_2O was mixed with Ne, Ar, Kr and Xe. We used the same noble gases in the third set of experiments, but this time we mixed them with synthetic air instead of N_2O. The total gas flow was fixed to 100 sccm throughout the experiments, and the flows of each individual gas are presented interchangeably as % and sccm.

It should be noted that a processor of the kind used here has several possible sources of parasitic air unintentionally entering the gas and liquid phases, such as seals and fittings in addition to the water itself and operational procedures. We took care to eliminate all of these until the yield of nitrite and nitrate was insignificant in the absence of a deliberately added source of nitrogen.

Due to degradation of the sonotrode, titanium powder residues could be found in the liquid samples. Samples were therefore filtered prior to chemical analysis in 10 mL batches using PES syringe filters with pore size 0.45 μm.

The liquid products were characterized by high-pressure ion chromatography (HPIC), using a Dionex Integrion HPIC system configured for reagent-free ion chromatography (IC). Ten standards were made using Reagecon Seven Anion Standard, which enables the quantification of fluorides, chlorides, nitrites, sulfates, borides, nitrates, and phosphates. The most and least diluted standards contained 0.002 and 10 mg L^{-1}, respectively, of both NO_2^- and NO_3^-. Unless otherwise specified, all data points in the figures are an average of three IC measurements.

Computational

The ORCA 5.0.1 program package[29–31] was used for the quantum chemical computations. All stationary points of the potential energy hypersurface (reactants, transition states, intermediates, and products) and minimum energy crossing points (MECP) between the diabatic potential energy surfaces were characterized by complete geometry optimizations. The computations were performed using density functional theory with the hybrid functional B3LYP, full-valence CASSCF and coupled cluster with singlets, doublets and perturbational triplets (CCSD(T)) in conjunction with the augmented Dunning correlation-consistent polarized quadruple-zeta (aug-cc-pVQZ) basis set.[32] The CASSCF calculations were subsequently corrected for dynamic correlation using FIC-NEVPT2.[33–36] Reactants, intermediates and products were characterized by analytic or numerical frequency calculations depending on the availability for each level of theory. All reactants and intermediates have positive definite Hessian matrices, while transition state structures have a single negative eigenvalue in their diagonalized force constant matrices. The calculations were compared with existing experimental and computational data using the ANL ATcT databases.[37,38]

Experimental results

The first series of experiments was aimed at finding the optimum ratio of O_2 in O_2/N_2 gas mixtures. The results are
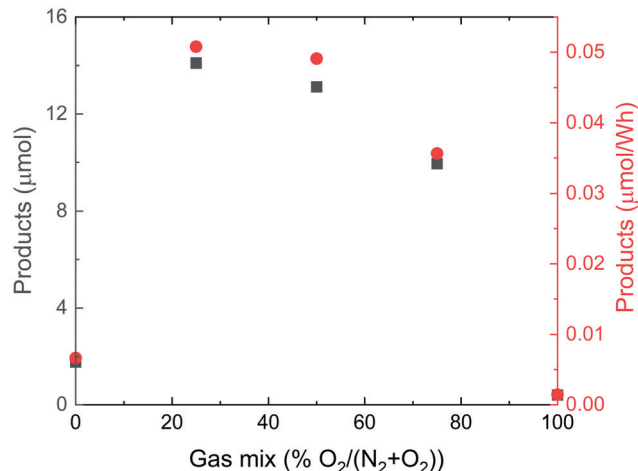

Fig. 1 The integrated amount of nitrate and nitrite produced (black squares) and the same amount relative to the energy dissipated into the system (red circles) as a function of the relative amount of O_2 in the N_2 + O_2 gas mixture, fed at 100 sccm. Some of the data points are overlapping.

presented in Fig. 1, which shows the total amount of NO_2^- and NO_3^- produced for each mixture investigated. Interestingly, a shallow maximum production is found for the gas mixture that resembles air the most.

Based on these findings, we decided to apply an $O_2:N_2$ ratio of 20:80 (synthetic air) for the second series of experiments, in which equal amounts of a noble gas and synthetic air were introduced into the water. The results are presented in Fig. 2. Significantly more products $(NO_2^- + NO_3^-)$ are formed by introducing Ar, Kr and Xe, and production increases noticeably down the group of noble gases.

A third series of measurements was made for variable mixtures of N_2O and Ar, Fig. 3. Maximum nitrate + nitrite production is observed around 10 sccm N_2O + 90 sccm Ar. This is consistent with the results of similar measurements
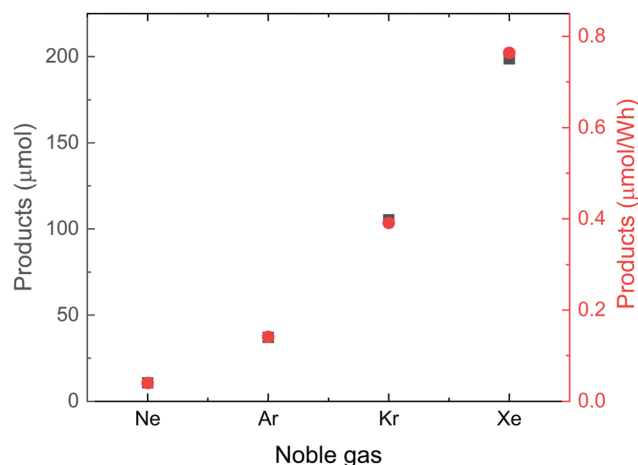

Fig. 2 The integrated amount of nitrate and nitrite produced after flowing a mixture of 50 sccm synthetic air and 50 sccm noble gas through the liquid sample before and during ultrasonication. Some of the data points are overlapping.
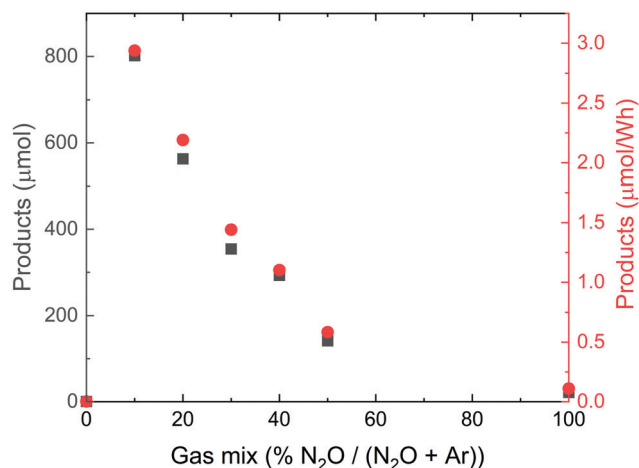
This journal is © the Owner Societies 2022

Phys. Chem. Chem. Phys., 2022, 24, 15357–15364 | 15359

Fig. 3 The integrated amount of nitrate and nitrite produced (black squares) and the same amount relative to the energy dissipated into the system (red circles) as a function of the relative amount of N_2O in the N_2O + Ar gas mixture, fed at 100 sccm. Some of the data points are overlapping.

performed by Hart and Henglein,[20] and Nikitenko and Seliverstov,[39] so this mixing ratio was applied for the following experiments with the other noble gases, see below.

Fig. 4 shows the results of the fourth and final series of measurements that were conducted for mixtures of N_2O/E (E = Ne, Ar, Kr, Xe), with 10% N_2O and 90% of the noble gas. Also in this case, a significant periodic trend Ne < Ar < Kr < Xe is observed.

Discussion

From Fig. 1 we estimate that the sum of nitrite and nitrate products in a 2:1 mixture of N_2 and O_2, in the absence of a noble gas, amounts to 13 μmol, which is 95% of that measured at the maximum of the curve, for synthetic air (4:1). In the presence of Ar (Fig. 2), after normalizing to the same total gas
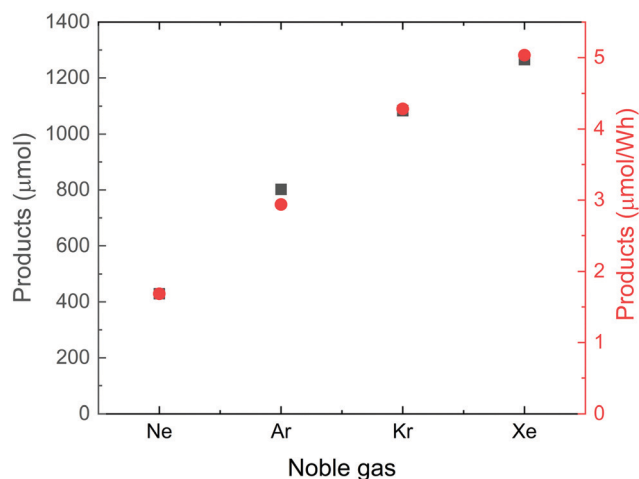

Fig. 4 The integrated amount of nitrate and nitrite produced for each noble gas after flowing mixtures of 10 sccm N_2O and 90 sccm noble gas mixtures through the liquid. Some of the data points are overlapping.

flow as in Fig. 2, the product yield increases to 2×35 μmol = 70 μmol. However, when we instead use N_2O (also having N:O = 2:1) as reactant, and also with Ar present, the yield increases to 10×800 μmol = 8000 μmol (Fig. 4), when normalized to the same reactant gas flow as used in the Fig. 1 experiments. For these considerations, we need to realize that N_2O is 20 times more soluble in water than O_2 and 40 times more soluble than N_2 (see ESI†). Therefore, if we assume that N_2 solubility is the limiting factor in the $N_2 + O_2$ case, this shows the amount of produced nitrite and nitrate should be 8000 μmol/40 = 200 μmol, approximately three times higher. In other words, when N_2O is used as reactant, the amount of products formed is three times higher than when an N_2/O_2 mixture with the same stoichiometric ratio is used. This rules out thermodynamic equilibrium in the two experiments. Although our simple analysis is not based on any systematic kinetic study, it is tempting based on the available data to hypothesize that nitrous oxide may be an intermediate during nitric oxide formation in the reaction between N_2 and O_2, *i.e.*,

$$N_2 + O_2 \rightarrow N_2O \rightarrow NO. \quad (6)$$
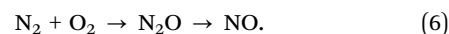
This was suggested already in 1950 by Virtanen, who wrote: "The aerobic fixation of nitrogen in ultrasonic fields leads to a nitrogen oxide, *e.g.*, NO or possibly N_2O. Which in fact is the first oxide formed is not known."[14,15] It still took some years before Hart, Fisher and Henglein in 1986 were able to observe N_2O in a sonochemical experiment, where they used isotopically labelled reactants and were able to account for the reaction mechanism in a semiquantitative manner.[21] However, only small amounts of N_2O were observed in their experiments. This was explained by a dynamic process where N_2O is both formed and destroyed in fast radical reactions. The hypothesis that N_2O actually is an intermediate during NO production is also consistent with the fact that nitrate formation is greatly enhanced in the presence of added oxygen gas,[16] as mentioned in the Introduction. This is the opposite of the effect of added O_2 for N_2/O_2, Fig. 1. In the same paper it also appears that the source of the reactive oxygen species in that study is primarily dissolved O_2 or N_2O, and that OH radicals produced from water by bond dissociation are of less importance, which is often considered to be the key reactive oxygen species in many sonochemical reactions.

The fact that reactivity increases down the group Ne < Ar < Kr < Xe is consistent with the results of the elegant sonoluminescence experiments reported from the laboratories of Suslick and Nikitenko.[12,23–27] We note that the observed trends in reactivity show good correlation with noble gas solubility. In the case of $N_2 + O_2$, the correlation is linear, while for N_2O it is slightly curved, see Fig. S1 and S2 in ESI.† Whether the correlations between solubility and reactivity relate to the number of bubbles created, the electron temperature of the transient plasma due to the ease of ionization or is coincidental—in the sense that most physical properties change monotonically down the group of noble gases can, of course, not be straightforwardly determined based on the present data. We will, despite this critical comment, relate the rest of our

15360 | *Phys. Chem. Chem. Phys.*, 2022, **24**, 15357–15364

This journal is © the Owner Societies 2022

discussion to the electron temperature scenario substantiated by the two named laboratories.

As already explained, a short-lived plasma is formed during bubble collapse upon sonication of a liquid. In general, a manifold of chemical reactions is involved in this high-energy event and in the following period as the liquid quickly approaches room temperature. The extremely fast temperature and pressure changes make a complete, quantitative description of the chemical system very demanding, if not essentially impossible. However, a great deal is known about the general features of plasma chemistry, irrespective of the plasma is formed in electric discharges, in flames, in shock waves from detonations, upon electromagnetic radiation, or by sonication. In the present context, a comprehensive and recent account of the chemistry in $N_2 + O_2$ plasmas by Guerra *et al.*[40] provides a good guide to this fascinating landscape. Just to describe the reactions between the numerous neutral and charged species formed from these two diatomic molecules alone (in the absence of water) the authors involve 198 different elementary reactions, each with a given rate coefficient. With humble recognition of the overall complexity, we will extend the simplified Zel'dovich model (eqn (4) and (5)) by including N_2O explicitly as an intermediate and relate this to the non-adiabatic high electron temperature regime advocated by Suslick and Nikitenko.

In doing so, we will first examine how energy rich electrons interact with O_2 and N_2, respectively, to provide atomization. From a thermodynamic perspective, since the bond dissociation energy of O_2 is half that of N_2 (498 *vs.* 945 kJ mol^{-1}), one could expect that this gives rise to more O atoms than N atoms. But in a plasma with a myriad of fast electrons the dominating process for atomization will be by electron-impact dissociation:

$$e^- + N_2 \rightarrow e^- + 2N \tag{7}$$

and

$$e^- + O_2 \rightarrow e^- + 2O. \tag{8}$$
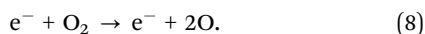
The cross sections for these processes, in which both the doublet and quartet states of and atomic nitrogen (7) and the singlet and triplet states of atomic oxygen (8) are produced, have been determined experimentally, and it turns out to be higher for N_2 than O_2 by 20–200% in the range 10–200 eV.[41,42] In synthetic air this would imply that initially there will be of the order of 10 times more N atoms than O atoms. Using this number, subsequent $N + O_2$ collisions will be more frequent than $O + N_2$ collisions in synthetic air by a factor of 2.5. We will therefore look closer at possible reactions between N and O_2 and have constructed the relevant potential energy diagram, Fig. 5, based on quantum chemical calculations.

It should be noted that none of the computational methods employed are able to fully describe all features of the systems studied. While CCSD(T) works very well for the minima and give values close to the experimental values with low T1 diagnostics, it does not handle the multireference character during bond-breaking in transition states as well and breaks down completely for the minimum energy crossing points
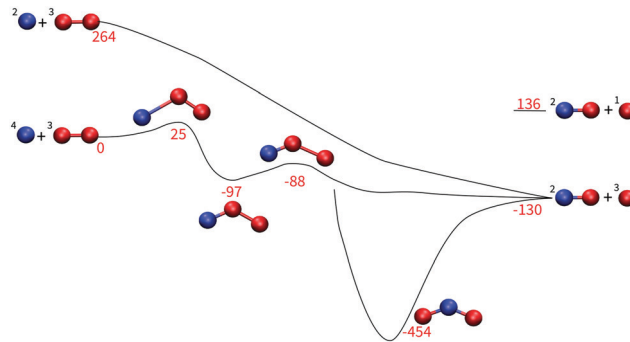

Fig. 5 Potential energy diagram for lowest energy reactions (all electronic doublet states) between N and O_2 obtained by B3LYP calculations, see text for description. All energies in kJ mol^{-1}.

(MECPs). On the other hand, CASSCF presumably handles the MECPs better, but it is less suited for *e.g.* N_2O as has been previously demonstrated.[43,44] B3LYP seems to handle both the stationary points and the MECPs somewhat well and is thus used throughout the discussion. Because of these discrepancies, we advise that the computed values are taken merely as qualitative. We also note that some of the experimental values used for comparison are not entirely trustworthy and some of the listed intermediates are debated whether they even exist as stable minima.[45–48] Comparisons of the different computational methods and experimental values are listed in the ESI.†

The left hand side of Fig. 5 shows two reactant states with the lowest quartet state of nitrogen atom, ^4S, with the doublet ^2D lying 264 kJ mol^{-1} higher in energy, compared to the spectroscopic value of 230 kJ mol^{-1}.[49] The right hand side displays two product states, with the lowest triplet state of oxygen atom, ^3P, with the singlet ^1D being 266 kJ mol^{-1} higher in energy, compared to the spectroscopic value of 190 kJ mol^{-1}.[49] Regarding the reaction mechanism, the potential energy surfaces of $N + O_2$ reactions have been studied in greater detail by others,[50–53] and here we limit ourselves to display only a few characteristic features relevant to the present context. Starting from the ground doublet reactant state ($^4N + {}^3O_2$), after passing a modest barrier of 25 kJ mol^{-1}, a local minimum corresponding to the peroxy radical NOO is reached. The existence of this species has been debated in the literature,[50] but both the aforementioned quantum chemical studies and a recent velocity-map imaging study[54] indicate that NOO corresponds to a local minimum albeit with a limited lifetime. Ultimately, the products $^2NO + {}^3O$ are formed after passing the submerged barrier at −88 kJ mol^{-1}. From Fig. 5 we also see that the same products are formed in a barrierless reaction from the electronically excited state $^2N + O_2$, while there is only a small barrier for $^2N + O_2 \rightarrow NO + {}^1O$. All the three essentially direct exothermic reactions therefore constitute efficient channels for forming NO, in accordance with the first Zel'dovich reaction (eqn (4)). In Fig. 5 we have also included nitrogen dioxide (ONO), which is the lowest energy point of the potential energy surface. There seems to be no other route from NOO to ONO other than *via* the $^2NO + {}^3O$ asymptote as
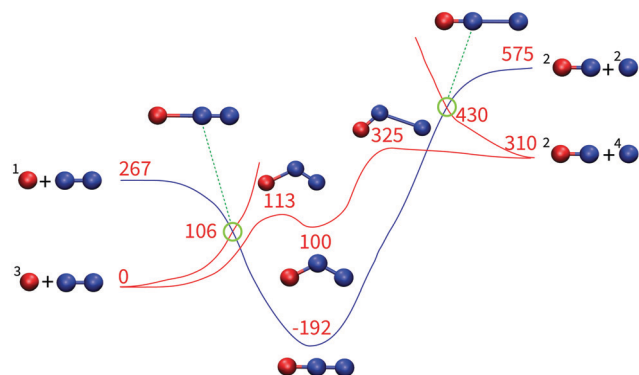
This journal is © the Owner Societies 2022

Phys. Chem. Chem. Phys., 2022, **24**, 15357–15364 | **15361**

Fig. 6 Potential energy diagram for lowest energy reactions (blue: electronic singlet state, red: electronic triplet state) between O and N_2 obtained by B3LYP calculations, see text for description. For linear geometries intersystem (singlet/triplet) crossing may occur at the points marked with green circles. As only lighter period 2 elements contribute to this reaction path, the spin–orbit coupling effect is small compared to the MECP barriers. All energies in kJ mol^{-1}.
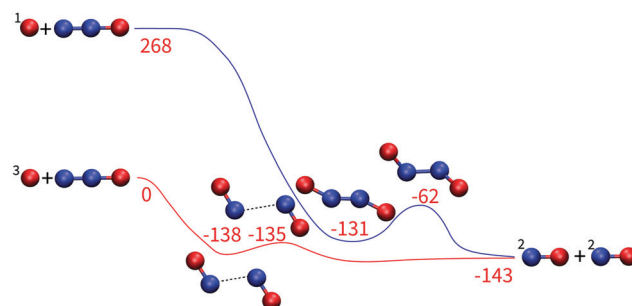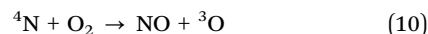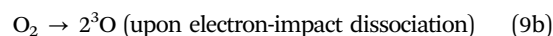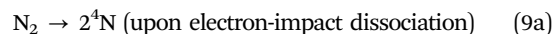

Fig. 7 Potential energy diagram for lowest energy reactions (blue: electronic singlet state, red electronic triplet state) between O and N_2O obtained by B3LYP calculations, see text for description. All energies in kJ mol^{-1}.

indicated in the diagram. On the other hand, this shows that NO is easily oxidized to NO_2 in direct reaction with ^3O once the temperature and the pressure allows for trapping this product by third body collisions.

The potential energy surfaces of N_2O have been surveyed in photodissociation[55–57] and electron-impact dissociation experiments,[58,59] and by quantum chemical calculations.[55,60,61] These studies provided the background for our own quantum chemical model displayed in Fig. 6.

From the energy diagram of Fig. 6 we see that the second Zel'dovich reaction (O + N_2 → NO + N, eqn (5)) is endothermic, irrespective of whether the reactant oxygen atom is the singlet or the triplet or whether the product nitrogen atom is the doublet or the quartet. Only at very high vibrational temperatures of N_2, any of the indicated channels will therefore be open. In addition, N atoms formed by electron-impact dissociation are more prevalent in a hot electron plasma than O atoms, see above, so we must conclude that the O + N_2 pathway to NO is clearly less important than the corresponding N + O_2 pathway discussed above. All this is consistent with the kinetic data collected and presented by Guerra et al.[40]

The global minimum of Fig. 6 corresponds to nitrous oxide, which exists en route to NO on the singlet surface. If the temperature is not too high or the pressure too low, this species may be trapped by third body collisions, which explains why it has been observed as an end product in sonochemical reactions of air, albeit in small quantities.[21] Alternatively, the metal residue produced by sonotrode disintegration may catalyze the spin inversion from the triplet to the singlet state to form and stabilize N_2O. Both the ease of electron-impact dissociation of N_2O[58,59] and its high reactivity with other species present (see below) make this species fragile in a plasma. Despite this, N_2O appears to play an important supporting role in the reactions studied here. In our sonochemical experiments using pure N_2O as reactant, we observed that this gives rise to more products when we react an N_2:O_2 mixture of the same

stoichiometry. Second, due to its vulnerability for electron-impact dissociation, it will be the main source for O atoms that in a next step may react with intact N_2O molecules to give NO. This is illustrated in Fig. 7, which we have obtained by quantum chemical calculation, capitalizing on the results from earlier studies.[58,62,63]
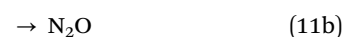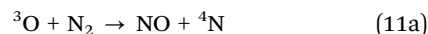
In agreement with the references cited immediately above we find that the reaction between triplet oxygen atom and N_2O is highly favorable, since this leads directly to two NO molecules in an exothermic, barrierless reaction via the elusive ON···NO complex. To which degree this species actually corresponds to a shallow potential energy minimum is questionable, since the computational methods give different answers to this. In any case this provides a rationale for the aforementioned "O" + N_2O pathway[17–22,39] now identifying the reactive oxygen species "O" to be ^3O. Whether the oxygen source is N_2O or O_2 seems to be of less importance than the observation that ^3O is the reactive species rather than OH radical formed by sonolysis of water. Fig. 7 also shows that ^1O also will react with N_2O, but with a more demanding mechanism, via the covalently bonded O=N–N=O intermediate that requires the passage of a transition state.

Conclusion

The energy diagrams in Fig. 5–7 help us suggest the major mechanism for formation of NO from N_2 and O_2 in the transient plasma formed upon bubble collapse, namely:

$$N_2 \rightarrow 2\,^4N \text{ (upon electron-impact dissociation)} \quad (9a)$$

$$O_2 \rightarrow 2\,^3O \text{ (upon electron-impact dissociation)} \quad (9b)$$

$$^4N + O_2 \rightarrow NO + {}^3O \quad (10)$$

Due to the relative cross sections for atomization and the relative natural abundance of the molecular components of air, there are fewer oxygen atoms produced than nitrogen atoms, and the obstacles due to energy barriers, the following sequence of elementary steps are of minor importance:

$$^3O + N_2 \rightarrow NO + {}^4N \quad (11a)$$

$$\rightarrow N_2O \quad (11b)$$

15362 | *Phys. Chem. Chem. Phys.*, 2022, **24**, 15357–15364

This journal is © the Owner Societies 2022

$$^{3}O + N_2O \rightarrow 2NO \qquad (12)$$

Therefore, N_2O turns out to be an intermediate during nitrogen oxidation, but seems to us to play a minor role in the overall picture.

The fact that the addition of noble gases increases product formation with the observed reactivity order Ne < Ar < Kr < Xe is best understood from the hot-electron model of Suslick and Nikitenko. Among the four noble gases, Xe is the most soluble and has the lowest ionization energy, giving rise to the highest flux of free electrons and most likely the most energetic ones. This in turn provides more atomization and thereby higher product yield.

A spectroscopic study of the sonoluminescence during NO_x formation would be valuable in elucidating the suggested mechanisms. However, our current experimental setup does not permit such experiments.

As a final comment, our nitrate + nitrite product yield is unimpressive from an industrial perspective, to state it mildly. Even in the presence of Xe the synthetic air mixture gives rise to modest 0.8 µmol W^{-1} h^{-1} (from Fig. 2) = 0.06 mg W^{-1} h^{-1} = 0.06 g kW^{-1} h^{-1} (based on the molecular mass of nitric acid). In comparison, the electric-arc Birkeland–Eyde process gives 60 g kW^{-1} h^{-1}.[5] A first step for improvement of sonochemical nitrogen oxidation would be to eliminate water using a non-volatile solvent, and consequently separate NO production from the following reaction steps (oxidation to nitrogen dioxide and hydrolysis). Virtanen noticed already seven decades ago that hydrogen is unavoidably present in water upon sonolysis, and therefore has an inhibitory effect on nitrate formation since it is a reductant.[14,15] More recent studies have shown that the low viscosity and considerable vapor pressure of water, even at room temperature, counteract fast energy release during bubble collapse and specifically introduce unproductive OH radicals.[17,18] The sonochemical process could also be improved by increasing the reactor pressure[64–66] and/or identifying more effective promotors than the noble gases that may facilitate nitrogen activation.

Author contributions

Thomas Qureishy: investigation, methodology, writing – review & editing. Sverre Løyland: investigation, writing – review & editing. Susanne J. Jørgensen: resources. Eline M. Færgestad: resources. Truls Norby: conceptualization, supervision, writing – review & editing, funding acquisition. Einar Uggerud: conceptualization, supervision, funding acquisition, writing – original draft, writing – review & editing.

Conflicts of interest

There are no conflicts to declare.

Acknowledgements

References

1 V. Smil, *Enriching the Earth, Fritz Haber, Carl Bosch, and the Transformation of World Food Production*, The MIT Press, Boston, 2001.

2 K. Birkeland, *Trans. Faraday Soc.*, 1906, **2**, 98–116.

3 S. Eyde, *J. R. Soc. Arts*, 1909, **57**, 568–576.

4 N. Cherkasov, A. O. Ibhadon and P. Fitzpatrick, *Chem. Eng. Process.*, 2015, **90**, 24–33.

5 K. H. R. Rouwenhorst, F. Jardali, A. Bogaerts and L. Lefferts, *Energy Environ. Sci.*, 2021, **14**, 2520–2534.

6 H. Cavendish, *Philos. Trans. R. Soc. London*, 1785, **75**, 372–384.

7 R. D. Hill, R. G. Rinker and H. D. Wilson, *J. Atmos. Sci.*, 1980, **37**, 179–192.

8 J. Yao, L. Chen, X. Chen, L. Zhou, W. Liu and Z. Zhang, *Ultrason. Sonochem.*, 2018, **42**, 42–47.

9 J. Lee, H. Sun, S.-k Im and M. Soo Bak, *J. Appl. Phys.*, 2017, **122**, 083303.

10 Y. B. Zel'dovich and Y. P. Raizer, in *Physics of Shock Waves and High-Temperature Hydrodynamic Phenomena*, ed. W. D. Hayes and R. F. Probstein, Dover Publications, Mineola, New York, 1967, ch. 8, vol. 2, pp. 564–573.

11 E. A. Neppiras, *Phys. Rep.*, 1980, **61**, 159–251.

12 K. S. Suslick and D. J. Flannigan, *Annu. Rev. Phys. Chem.*, 2008, **59**, 659–683.

13 H. Schultes and H. Gohr, *Angew. Chem.*, 1936, **49**, 420–423.

14 A. I. Virtanen and N. Ellfolk, *Acta Chem. Scand.*, 1950, **4**, 93–102.

15 A. I. Virtanen and N. Ellfolk, *J. Am. Chem. Soc.*, 1950, **72**, 1046–1047.

16 P. K. Supeno, *Ultrason. Sonochem.*, 2000, **7**, 109–113.

17 D. Lohse, M. P. Brenner, T. F. Dupont, S. Hilgenfeldt and B. Johnston, *Phys. Rev. Lett.*, 1997, **78**, 1359–1362.

18 Y. T. Didenko and K. S. Suslick, *Nature*, 2002, **418**, 394–397.

19 A. Henglein, *Z. Naturforsch., B: Anorg. Chem., Org. Chem.*, 1985, **40b**, 100–107.

20 E. J. Hart and A. Henglein, *J. Phys. Chem.*, 1986, **90**, 5992–5995.

21 E. J. Hart, C. H. Fischer and A. Henglein, *J. Phys. Chem.*, 1986, **90**, 5989–5991.

22 E. J. Hart and A. Henglein, *J. Phys. Chem.*, 1985, **89**, 4342–4347.

This journal is © the Owner Societies 2022

Phys. Chem. Chem. Phys., 2022, **24**, 15357–15364 | **15363**

23 D. J. Flannigan and K. S. Suslick, *Phys. Rev. Lett.*, 2005, **95**, 044301.

24 N. C. Eddingsaas and K. S. Suslick, *J. Am. Chem. Soc.*, 2007, **129**, 3838–3839.

25 K. S. Suslick, N. C. Eddingsaas, D. J. Flannigan, S. D. Hopkins and H. Xu, *Acc. Chem. Res.*, 2018, **51**, 2169–2178.

26 R. Pflieger, H.-P. Brau and S. I. Nikitenko, *Chem. – Eur. J.*, 2010, **16**, 11801–11803.

27 A. A. Ndiaye, R. Pflieger, B. Siboulet and S. I. Nikitenko, *Angew. Chem., Int. Ed.*, 2013, **52**, 2478–2481.

28 S. I. Nikitenko and R. Pflieger, *Ultrason. Sonochem.*, 2017, **35**, 623–630.

29 F. Neese, *Wiley Interdisc. Rev.: Comput. Mol. Sci.*, 2012, **2**, 73–78.

30 F. Neese, *Wiley Interdisc. Rev.: Comput. Mol. Sci.*, 2018, **8**, e1327.

31 F. Neese, F. Wennmohs, U. Becker and C. Riplinger, *J. Chem. Phys.*, 2020, **152**, 224108.

32 T. H. Dunning, *J. Chem. Phys.*, 1989, **90**, 1007–1023.

33 Y. Guo, K. Sivalingam, E. F. Valeev and F. Neese, *J. Chem. Phys.*, 2017, **147**, 064110.

34 C. Angeli, R. Cimiraglia and J.-P. Malrieu, *Chem. Phys. Lett.*, 2001, **350**, 297–305.

35 C. Angeli, R. Cimiraglia and J.-P. Malrieu, *J. Chem. Phys.*, 2002, **117**, 9138–9153.

36 C. Angeli, R. Cimiraglia, S. Evangelisti, T. Leininger and J. P. Malrieu, *J. Chem. Phys.*, 2001, **114**, 10252–10264.

37 B. Ruscic, R. E. Pinzon, M. L. Morton, G. von Laszevski, S. J. Bittner, S. G. Nijsure, K. A. Amin, M. Minkoff and A. F. Wagner, *J. Phys. Chem. A*, 2004, **108**, 9979–9997.

38 B. Ruscic, R. E. Pinzon, G. v Laszewski, D. Kodeboyina, A. Burcat, D. Leahy, D. Montoy and A. F. Wagner, *J. Phys.: Conf. Ser.*, 2005, **16**, 561–570.

39 S. I. Nikitenko and A. F. Seliverstov, *Russ. Chem. Bull.*, 2000, **49**, 2077–2079.

40 V. Guerra, A. Tejero-del-Caz, C. D. Pintassilgo and L. L. Alves, *Plasma Sources Sci. Technol.*, 2019, **28**, 073001.

41 P. C. Cosby, *J. Chem. Phys.*, 1993, **98**, 9544–9553.

42 P. C. Cosby, *J. Chem. Phys.*, 1993, **98**, 9560–9569.

43 D.-Y. Hwang and A. M. Mebel, *Chem. Phys.*, 2000, **259**, 89–97.

44 J. M. L. Martin and T. J. Lee, *J. Chem. Phys.*, 1993, **98**, 7951–7957.

45 H. A. Duarte, E. Proynov and D. R. Salahub, *J. Chem. Phys.*, 1998, **109**, 26–35.

46 E. A. Wade, J. I. Cline, K. T. Lorenz, C. Hayden and D. W. Chandler, *J. Chem. Phys.*, 2002, **116**, 4755–4757.

47 K. A. Nguyen, M. S. Gordon, J. A. Montgomery, Jr. and H. H. Michels, *J. Phys. Chem.*, 1994, **98**, 10072–10078.

48 M. A. Vincent, I. H. Hillier and L. Salsi, *Phys. Chem. Chem. Phys.*, 2000, **2**, 707–714.

49 C. E. Moore and J. W. Gallagher, *Tables of spectra of hydrogen, carbon, nitrogen, and oxygen atoms and ions*, 1993.

50 S. P. Walch, *J. Chem. Phys.*, 1995, **102**, 4189–4192.

51 M. Braunstein and J. W. Duff, *J. Chem. Phys.*, 2000, **113**, 7406–7413.

52 V. Kurkal, P. Fleurat-Lessard and R. Schinke, *J. Chem. Phys.*, 2003, **119**, 1489–1501.

53 M. González, I. Miquel and R. Sayós, *Chem. Phys. Lett.*, 2001, **335**, 339–347.

54 B. A. Laws, S. J. Cavanagh, B. R. Lewis and S. T. Gibson, *J. Phys. Chem. Lett.*, 2017, **8**, 4397–4401.

55 P. Felder, B. M. Haas and J. Robert Huber, *Chem. Phys. Lett.*, 1991, **186**, 177–182.

56 T. F. Hanisco and A. C. Kummel, *J. Phys. Chem.*, 1993, **97**, 7242–7246.

57 D. Yuan, S. Yu, T. Xie, W. Chen, S. Wang, Y. Tan, T. Wang, K. Yuan, X. Yang and X. Wang, *J. Phys. Chem. A*, 2018, **122**, 2663–2669.

58 D. A. Shutov, S.-Y. Kang, K.-H. Baek, K.-S. Suh and K.-H. Kwon, *J. Korean Phys. Soc.*, 2009, **55**, 1836–1840.

59 K. Katsonis and C. Berenguer, *Int. J. Aerosp. Eng.*, 2013, **2013**, 737463.

60 J. A. Schmidt, M. S. Johnson, U. Lorenz, G. C. McBane and R. Schinke, *J. Chem. Phys.*, 2011, **135**, 024311.

61 R. Schinke, *J. Chem. Phys.*, 2011, **134**, 064313.

62 T. Takayanagi and H. Akagi, *Chem. Phys. Lett.*, 2002, **363**, 298–306.

63 R. Li and R. E. Continetti, *J. Phys. Chem. A*, 2002, **106**, 1183–1189.

64 I. G. Polotskii, *Zh. Obshch. Khim.*, 1947, **6**, 1048–1054.

65 K. Gaddam and H. M. Cheung, *Ultrason. Sonochem.*, 2001, **8**, 103–109.

66 M. Haïssinsky, R. Klein and P. Rivayrand, *J. Chim. Phys. Phys.-Chim. Biol.*, 1962, **59**, 611–622.